Received: 15 February 2021 | Revised: 18 May 2021 | Accepted: 1 June 2021

DOI: 10.1002/hbm.25558

RESEARCH ARTICLE

WILEY

# Characterizing white matter alterations subject to clinical laterality in drug-naïve de novo Parkinson's disease

Yiming Xiao[1,2] | Terry M. Peters[3,4,5] | Ali R. Khan[3,4,5,6]

[1]Department of Computer Science and Software Engineering, Concordia University, Montreal, Canada

[2]PERFORM Centre, Concordia University, Montreal, Canada

[3]Imaging Research Laboratories, Robarts Research Institute, Western University, London, Canada

[4]Department of Medical Biophysics, Schulich School of Medicine and Dentistry, Western University, London, Canada

[5]School of Biomedical Engineering, Western University, London, Canada

[6]The Brain and Mind Institute, Western University, London, Canada

**Correspondence**
Yiming Xiao, Department of Computer Science and Software Engineering, Concordia University, 1455 Boulevard de Maisonneuve O., Montreal, Quebec, Canada H3G 1M8.
Email: yiming.xiao@concordia.ca

**Funding information**
brainsCAN fellowship; Canadian Institutes of Health Research fellowship

## ABSTRACT

Parkinson's disease (PD) is a progressive neurodegenerative disorder that is characterized by a range of motor and nonmotor symptoms, often with the motor dysfunction initiated unilaterally. Knowledge regarding disease-related alterations in white matter pathways can effectively help improve the understanding of the disease and propose targeted treatment strategies. Microstructural imaging techniques, including diffusion tensor imaging (DTI), allows inspection of white matter integrity to study the pathogenesis of various neurological conditions. Previous voxel-based analyses with DTI measures, such as fractional anisotropy and mean diffusivity have uncovered changes in brain regions that are associated with PD, but the conclusions were inconsistent, partially due to small patient cohorts and the lack of consideration for clinical laterality onset, particularly in early PD. Fixel-based analysis (FBA) is a recent framework that offers tract-specific insights regarding white matter health, but very few FBA studies on PD exist. We present a study that reveals strengthened and weakened white matter integrity that is subject to symptom laterality in a large drug-naïve de novo PD cohort using complementary DTI and FBA measures. The findings suggest that the disease gives rise to tissue degeneration and potential re-organization in the early stage.

**KEYWORDS**
asymmetry, diffusion MRI, DTI metrics, fixel-based analysis, microstructure, Parkinson's disease, voxel-based analysis, white matter

## 1 | INTRODUCTION

Parkinson's disease (PD) is a progressive neurodegenerative disorder characterized by the loss of dopaminergic neurons in the midbrain. Although the disease primarily affects the patient's motor functions, it can also induce a range of nonmotor symptoms, such as depression and sleep disturbance, as a result of modifications in brain connectivity (Ji et al., 2019). Precise knowledge regarding disease-related changes in white matter pathways can effectively help improve the understanding of the disease and its treatment strategy. Microstructural imaging techniques, including diffusion tensor imaging (DTI), allow inspection of white matter integrity to study the pathogenesis and progression of neurological conditions.

In the past, a number of studies have investigated brain tissue changes in PD using DTI techniques (Atkinson-Clement, Pinto,

Terry M. Peters and Ali R. Khan share the senior authorship.

Eusebio, & Coulon, 2017; Zhang & Burock, 2020). Compared with morphometric analysis (Sarasso, Agosta, Piramide, & Filippi, 2020; Xiao et al., 2014) that intends to characterize macroscopic anatomical changes, quantitative MRI (qMRI) measures have shown superior sensitivity in detecting tissue degeneration due to the disease. More specifically, voxel-based analyses (VBA) with DTI measures, such as fractional anisotropy (FA) and mean diffusivity (MD) have revealed PD-related tissue alteration patterns, but unfortunately these findings were often inconsistent across studies, especially within white matter regions, partially due to smaller patient cohorts, sensitivity to heterogeneity in patient groups (e.g., variations in disease stages, symptoms, and treatment history), and MRI parameters (e.g., number of gradient directions in diffusion-weighted imaging/DWI sequences). In their meta-analysis of 39 studies, Atkinson-Clement et al. (2017) show that cellular degeneration measured as reduced FA and elevated MD exist more consistently within the substantia nigra, corpus callosum, and the cingulate and temporal cortices in PD patients.

Based on diffusion MRI, fixel-based analysis (FBA) (Raffelt et al., 2017) is a relatively recent method that offers tract-specific insights regarding white matter health. Instead of the more simplistic DTI model, FBA models fiber populations within one voxel (called a *fixel*) through functions of fiber orientation, and derives quantitative metrics in both macroscopic and microscopic scales to characterize white matter fibers, including fiber cross-section (FC), fiber density (FD), and the combined measure of fiber density and cross-section (FDC). Among these, FC reflects the macroscopic changes of the fiber bundles in terms of their cross-sectional areas; FD measures the density of fibers within a fiber bundle; and FDC evaluates the combined impact of FC and FD in white matter tracts. In contrast to conventional voxel-based analyses with DTI measures, which fail to handle fiber-crossing within voxels, FBA allows more interpretable results by identifying specific fiber tracts that are relevant to the designated study. Since its debut, this technique has demonstrated good specificity, sensitivity, and reliability in various applications, including natural aging (Choy et al., 2020), Alzheimer's disease (Mito et al., 2018), stroke (Egorova et al., 2020), traumatic brain injury (Wallace et al., 2020), and mental disorders (Lyon et al., 2019).

To date, very few have attempted to characterize white matter alterations as a result of PD using FBA. The existing studies (Li et al., 2020; Rau et al., 2019; Zarkali et al., 2020) primarily focus on early-stage patients, who have started drug treatment. More specifically, Rau et al. (2019) conducted a longitudinal analysis over a follow-up period of 40 months for 50 PD patients. Their results suggest degeneration in the splenium of the corpus callosum (CC), measured by reduced FC and FDC, as a typical alteration of PD. In addition to the CC, both decrease and increase of FBA-based metrics have been detected in various white matter tracts between different follow-up points. However, no significant differences were found between healthy controls and PD patients at the baseline with DTI or FBA-based metrics. Overall, fixel-based metrics were correlated with the worsening of a 39-item PD questionnaire, Unified Parkinson's Disease Rating Scale (UPDRS), and activity of daily living. Later, Li et al. (2020) compared fixel-based measures among 41 PD patients in the early stage [Hoehn and Yahr (H&Y) =1–1.5], 57 PD patients in the middle stage (H&Y = 2–2.5), and 76 healthy controls. The comparison demonstrated significant differences in FD of the corticospinal tract (CST) and FC of the superior cerebral peduncle (SCP) among the three groups, with the mean FD value of the CST higher in the PD groups than healthy controls. In addition, they also found a correlation between reduced FD of the CC and the deterioration of motor and psychiatric symptoms. Finally, Zarkali et al. (2020) investigated Parkinson hallucination and visual dysfunction with FBA, and discovered lower FC and FDC within the splenium of the CC, as well as lower FC in the left posterior thalamic radiata for patients with Parkinson hallucinations than those without the symptom.

It is known that motor symptoms of PD usually initiate unilaterally and then progress to both sides of the body, and evidence has linked the laterality of motor symptoms onset with the prognosis of the disease (Baumann, Held, Valko, Wienecke, & Waldvogel, 2014; Munhoz et al., 2013). For example, patients with the initial motor symptoms onset on the right-side are associated with faster disease progression (Baumann et al., 2014), and those with left-side onset were reported to have longer disease duration (Munhoz et al., 2013). Since the clinical laterality onset may impact the brain hemispheres differently (Scherfler et al., 2012; Shang et al., 2020), this factor should be fully considered in relevant neuroimage analyses of PD, especially when involving patients at the early stages of the disorder. Unfortunately, in a majority of current image-based studies, the asymmetric development of PD is frequently overlooked. Besides the pitfall of limited patient cohorts in the analysis, the lack of consideration for laterality may have also contributed to the inconsistency in the findings of disease-related tissue changes, thus preventing a clear depiction of pathogenesis of the disease. Therefore, an investigation based on a large PD cohort, with an emphasis on the clinical laterality onset should better elucidate the relationship between the development of PD and the associated alterations in white matter integrity. Furthermore, a comparison between FBA and VBA with DTI-measures based on the same cohort can help consolidate the findings with different analytical approaches. These are expected to be instrumental to further decode the disease mechanism and search for effective biomarkers for PD.

In this study, we characterize the status of white matter health in a large cohort of drug-naïve de novo PD patients with respect to the laterality onset of motor symptoms using fixel-based analysis for the first time. From the public Parkinson's Progression Markers Initiative (PPMI) database, 141 patients were compared against 62 sex-matched and age-matched healthy controls, as well as within the cohort to reveal strengthened and weakened white matter tracts, subject to the clinical laterality onset. In addition, we also compared the results from FBA to VBA with DTI metrics, which further support the findings from FBA, while offering complementing insights.

## 2 | MATERIALS AND METHODS

### 2.1 | Participants

For the study, 141 drug-naïve *de novo* PD patients (age = 61 ± 9 years, 51 females) having motor symptoms of unilateral dominance and 62 sex-matched and age-matched healthy subjects (age = 61 ± 10 years, 22 females) were obtained from the Parkinson's Progression Markers Initiative database (www.ppmi-info.org/data), which is an ongoing multicenter study consisting of clinical evaluation, genetic information, bio-samples, and imaging data for the goal of identifying disease biomarkers. The up-to-date information on the study can be found at www.ppmi-info.org. At each participating PPMI site, written informed consent was obtained from all participants in the study. For the investigation, we included subjects who have T1w, T2w, and DWI images with the minimum age of 30 years from the database, and the patient data were collected from the baseline visits ($N = 152$). Any subjects ($N = 8$) with poor image quality by visual inspection were removed from the collection. All included PD patients have received clinical assessments, including the UPDRS for their symptoms and are at H&Y stage I or II without prior pharmaceutical treatment. Among these patients, 62 have motor symptoms more dominant on the left side and 79 on the right side. Patients affected by the motor dysfunction equally on both sides ($N = 3$) were excluded from the study. For easy annotation, we will refer the PD patients with left-dominant symptoms as *LPD* and those with right-dominant symptoms as *RPD*. From the clinical evaluations, the described study focuses on the UPDRS-I (nonmotor experience of daily living), UPDRS-III (motor function examination), total UPDRS (the composite of motor and nonmotor symptom evaluations), the Geriatric Depression Scale (GDS), and REM Sleep Behavior Disorder Screening Questionnaire Score (RBDSQ). They cover motor and nonmotor symptoms of PD that are of particular interest in the early stage of the disease. The detailed demographic information of the subjects and the symptom evaluations are detailed in Table 1. The same information with respect to the dominant side of motor symptoms is listed in Table 2. Statistical tests were performed in each table to assess the differences in the demographic and clinical information between groups.

**TABLE 1** Demographics of Parkinson's disease and healthy subjects

| | PD ($n = 141$) | HC ($n = 62$) | *p*-value |
|---|---|---|---|
| Age | 61.7 ± 8.9 | 61.4 ± 9.8 | .929[a] |
| Sex | 51 F and 90 M | 22 F and 40 M | .925[b] |
| H&Y | 1.6 ± 0.5 | NA | NA |
| UPDRS I | 5.1 ± 3.8 | 2.4 ± 3.3 | $<1.0 \times 10^{-7}$[c*] |
| UPDRS III | 20.8 ± 9.0 | 0.6 ± 1.3 | $<1.0 \times 10^{-29}$[c*] |
| Total UPDRS | 31.4 ± 13.3 | 3.3 ± 3.8 | $<1.0 \times 10^{-28}$[c*] |
| GDS | 2.3 ± 2.5 | 1.5 ± 2.8 | .0014[c*] |
| RBDSQ | 3.9 ± 2.5 | 2.9 ± 2.3 | .0049[c*] |

*Note:* Group differences were evaluated using statistical tests (a = Kruskal-Wallis test, b = Chi-square test, and c = Wilcoxon rank sum test), and *p-values* lower than .05 were considered significant (annotated with *).

**TABLE 2** Demographics of PD patients with left dominant and right dominant symptoms

| | Left dominant (n = 62) | Right dominant (n = 79) | *p*-value |
|---|---|---|---|
| Age | 59.8 ± 8.8 | 63.2 ± 8.8 | .024[a*] |
| Sex | 28 F and 34 M | 23 F and 56 M | .049[b*] |
| H&Y | 1.6 ± 0.5 | 1.5 ± 0.5 | .177[c] |
| UPDRS I | 5.2 ± 3.5 | 5.1 ± 4.0 | .702[c] |
| UPDRS III | 22.2 ± 9.1 | 19.7 ± 8.8 | .114[c] |
| Total UPDRS | 32.4 ± 12.3 | 30.6 ± 14.0 | .349[c] |
| GDS | 2.6 ± 2.6 | 2.1 ± 2.5 | .156[c] |
| RBDSQ | 3.8 ± 2.1 | 4.0 ± 2.7 | .945[c] |

*Note:* Group differences between left and right dominant PD groups were evaluated using statistical tests (a = Kruskal-Wallis test, b = Chi-square test, and c = Wilcoxon rank sum test), and *p-values* lower than 0.05 were considered significant (annotated with *).

### 2.2 | Imaging protocols and preprocessing

For each subject included in the study, we acquired full brain T1w and T2w structural MRI volumes and diffusion MRI scans from the PPMI database. The T1w images were obtained using a magnetization-prepared rapid acquisition gradient echo (MPRAGE) protocol (TE = 2.98 ms, TR = 2,300 ms, flip angle = 9°, and resolution = $1 \times 1 \times 1$ mm$^3$). The T2w MRIs have an in-plane resolution of $1 \times 1$ mm$^2$ and slice thickness of 2–3 mm. The diffusion-weight imaging (DWI) data were acquired using the following parameters: TE = 88 ms, TR = 900 ms, 64 gradient directions, *b*-values = 1,000s/mm$^2$, and resolution = $2 \times 2 \times 2$ mm$^3$. For the DWI sequence, one $B_0$ volume was acquired for each scan. The detailed MRI protocols can be found on the PPMI website (http://www.ppmi-info.org/study-design/research-documents-and-sops/).

Both T1w and T2w structural images were pre-processed with nonlocal mean image denoising (Manjon, Coupe, Marti-Bonmati, Collins, & Robles, 2010), nonuniformity correction using the N4 algorithm (Tustison et al., 2010), and intensity standardization. The brain mask was computed from T1w MRI using BeAST (Eskildsen et al., 2012), and T2w volumes were rigidly registered to the corresponding T1w images and resampled to $1 \times 1 \times 1$ mm$^3$ resolution. DWI scans were processed with denoising (Veraart et al., 2016), unringing, eddy current correction (Andersson & Sotiropoulos, 2016), motion and distortion correction, and finally bias field correction (Tustison et al., 2010). More specifically, susceptibility-related distortion in DWI scans was corrected by first obtaining the deformation fields from nonlinear registration between $B_0$ and T2w images in the phase encoding direction of DWI, and then applying the resulting deformation to the entire DWI series. The rest of the DWI pre-processing was performed using the MRtrix3 package (Tournier et al., 2019).

## 2.3 | Fixel-based analysis

We use the single-shell 3-tissue constrained spherical deconvolution (SS3T-CSD) algorithm (Dhollander, Raffelt, & Connelly, 2016) implemented in MRtrix3 (www.mrtrix.org) to conduct fixel-based analysis for our investigation. The algorithm can resolve white matter fiber orientation distributions (FODs) from single-shell diffusion MRI data while accounting for gray matter and cerebrospinal fluid (CSF) compartments. With the pre-processed DWI volumes, we obtained the FODs for each subject. In total, we conducted the following five groups of studies to characterize the white matter integrity using FBA, with the consideration of clinical laterality onset.

### 2.3.1 | FBA study 1

The FOD images from the LPD patients were left–right flipped while those from the rest of the patients and healthy controls were kept the same. This way, the clinical laterality onset of the patient population is kept on the right side of the body, and fixel-based metrics were compared between the PD and healthy groups.

### 2.3.2 | FBA study 2

With the clinical laterality onset aligned to the right, we took the data from all PD patients in *FBA Study 1*, and correlated the fixel-based metrics with the clinical scores UDPRS-I, UPDRS-III, total UPDRS, GDS, and RBDSQ.

### 2.3.3 | FBA study 3

The left-dominant and right-dominant patients were separated into two groups. The fixel-based metrics of each group were compared against those of the healthy controls.

### 2.3.4 | FBA study 4

The left-dominant and right-dominant patients were separated into two groups. Within each group, clinical evaluations, including UDPRS-I, UPDRS-III, total UPDRS, GDS, and RBDSQ, were correlated with the fixel-based metrics.

### 2.3.5 | FBA study 5

With the FOD images from the LPD patients left–right mirrored, we took all PD patients in FBA Study 1, and compared the fixel-based metrics between LPD and RPD cohorts to reveal their differences.

For each study, a study-specific template was created from all relevant subjects by using group-wise diffeomorphic nonlinear registration based on FODs at $1.3 \times 1.3 \times 1.3\ mm^3$ resolution. Then, the FOD image of each subject in the respective study was nonlinearly registered to the template, and the deformation fields were saved. A whole-brain tractogram with 2 million streamlines was generated by first obtaining an initial tractogram with 20 million streamlines using the probabilistic tractography algorithm, iFOD2 (Tournier, Calamante, & Connelly, 2010) on the population-averaged FOD template and then filtering the result with the spherical deconvolution informed filtering of tractograms (SIFT) algorithm (Smith, Tournier, Calamante, & Connelly, 2013), to reduce false positive streamlines. In the template space, fixel-based measures of FD and FC were computed within each voxel for all subjects of interest, and their combined measure, FDC, was obtained by multiplying FC and FD. Note that for statistical tests, the logarithm of FC was used instead of the raw value to ensure the data were normally distributed and centered around zero. The generalized linear model (GLM) was used to test the hypotheses of each study, and the connectivity-based fixel enhancement (CFE) (Raffelt et al., 2015) was employed to identify fixel metrics that are associated with the factors to be tested. For all studies, the effects of sex and age were modeled as covariates and controlled for all the tests. Here, nonparametric permutation testing (Nichols & Holmes, 2002) based on 10,000 random shuffles was used to account for multiple comparisons. Family-wise error (FWE) corrected $p$-value <.05 was used to determine the statistical significance. Results with fewer than 10 fixels that showed statistical significance were not considered meaningful and thus not reported. The Johns Hopkins University (JHU) white matter tract atlas (Mori et al., 2008) was used to help guide the identification of relevant white matter tracts.

## 2.4 | Voxel-based analysis with diffusion tensor imaging metrics

To complement the results of fixel-based analysis with more commonly used measures of white matter integrity, we performed voxel-based analyses with fractional anisotropy and mean diffusivity for the same population. After DWI preprocessing, we calculated FA and MD maps for each participant using *FMRIB's Diffusion Toolbox* (FDT, part of FSL). Each individual participant's FA and MD maps were then transformed to the respective template space, using the corresponding warps generated from FBA in Section 2.3. We then performed voxel-based analysis in the template space using the GLM. The JHU white matter tract atlas (Mori et al., 2008) was used to constrain the region of interest (ROI) for the analysis and to help guide the identification of relevant white matter tracts. Similar to FBA, nonparametric permutation testing and FWE corrected $p$-values were used to reveal significant results (corrected $p$-value <.05). The effects of sex and age were modeled as covariates and controlled for all the studies.

For voxel-based analysis, we also conducted five groups of studies, following the same strategies for FBA in Section 2.3. However, instead of testing fixel-based metrics, FA and MD values were

analyzed instead. With the correspondence to the respective FBA studies, we denote the sub-studies for DTI metrics as *VBA study 1–5*.

## 3 | RESULTS

### 3.1 | Fixel-based analysis

The results of fixel-based analysis are shown in Figures 1–6. For the studies that compare PD versus healthy groups, the white matter tracts with statistical significance were segmented from the whole brain tractogram and were colored by the effect size as a percentage relative to the healthy control mean. Similarly, when comparing LPD versus RPD, the significant tracts were colored by the effect size as a percentage relative to the LPD mean. For the rest of results that associate clinical assessments and fixel-based metrics, the associated FWE corrected *p*-values were used to color the significant tracts. Note that for each figure, we used pink for the person icon to signify experiments that used mirrored LPD images, and green for those that did not.

With *FBA Study 1*, we compare the fixel-based measures between PD patients and healthy controls after aligning the symptom dominant side to the right side of the body. The results are shown in Figure 1, with both lower and higher fixel-based metrics in PD brains. More specifically, we have observed higher FC and FDC in a number of white matter tracts in the right hemisphere, including the posterior limb of internal capsule, cingulum, corticospinal tract, and superior cerebellar peduncles. In the left hemisphere, there was higher FDC in the anterior limb of internal capsule. Finally, the left cingulum exhibited lower FD in PD patients. The results of *FBA Study 2* are shown in Figure 2. With the symptom dominant side aligned, we observed that the GDS score was inversely correlated with FD in the left stria terminalis and FDC in superior cerebellar peduncle.

In *FBA Study 3* and *FBA Study 4*, the PD cohort was divided into the left-dominant and right-dominant groups. When investigating the differences between each PD sub-cohort and healthy controls in *FBA Study 3*, higher FC in the right superior cerebellar peduncle and the cerebellum was observed in RPD (see Figure 3) while no statistically significant results were detected for LPD versus healthy subjects. When inspecting the association with clinical scores for the LPD sub-cohort (see Figure 4), we found that there was a negative correlation between FC in the right dentatothalamic tract and the RBDSQ evaluation. On the other hand, for RPD (see Figure 5), higher GDS was associated with lower FD in the left stria terminalis and elevated FC in the splenium of the corpus callosum and fornix.

In Figure 6, we compared the LPD and RPD cohorts in *FBA Study 5* with the scans of LPD subjects left–right mirrored so that the more affected side is aligned to the right side of the body. In general, the tracts with higher and lower measures in RPD than LPD were symmetric between hemispheres. More specifically, the RPD cohort had higher FC in the left corticospinal tract, right posterior thalamic radiation, and right anterior limb of internal capsule while lower FC occurred in the same tracts of the opposite hemisphere. For FD, the metric was lower for RPD in the corticospinal tract and cingulum in the right hemisphere, and in the anterior limb of internal capsule, superior cerebellar peduncle, and splenium of corpus callosum in the left hemisphere. In terms of FDC, the measure was higher in RPD in left posterior limb of internal capsule, left superior cerebellar

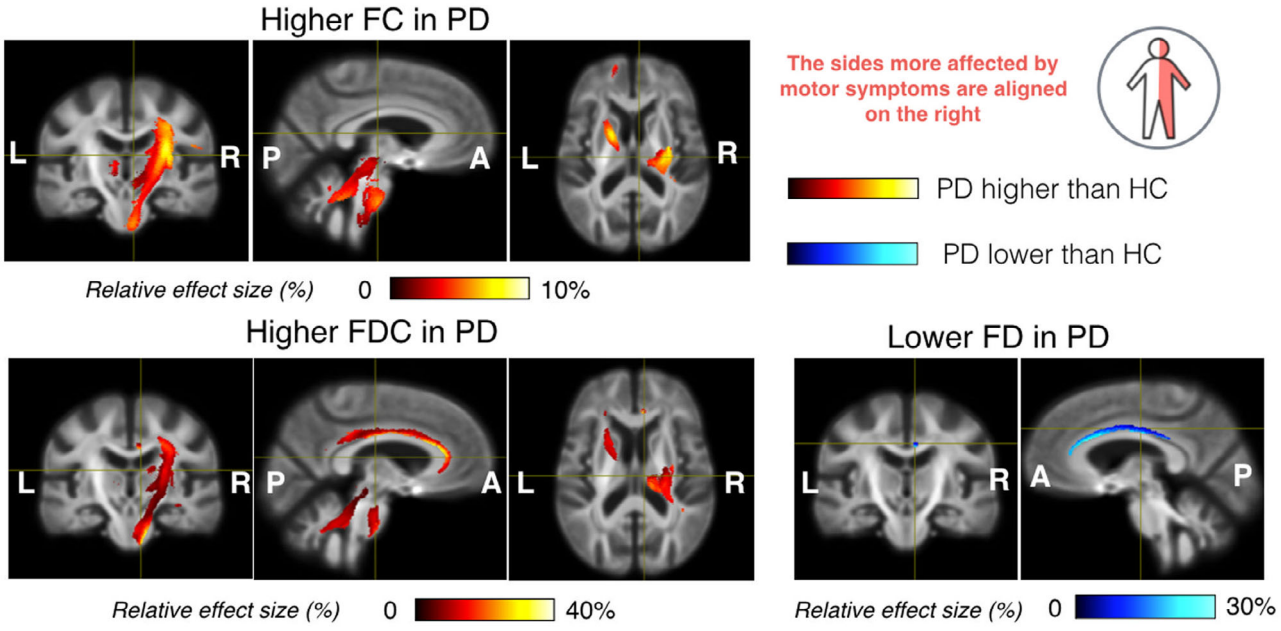


**FIGURE 1** Comparison of fixel-based metrics (FC, FD, and FDC) between PD and healthy groups after aligning laterality of symptom onset (*FBA Study-1*). Significant fiber tracts of fixel-based metrics (FWE-corrected $p < .05$) are overlaid on the group-averaged brain template, and the fiber tracts are colored by the percentage of effect size in PD group relative to the healthy group mean. In each image group, the cross-hair points at the same location

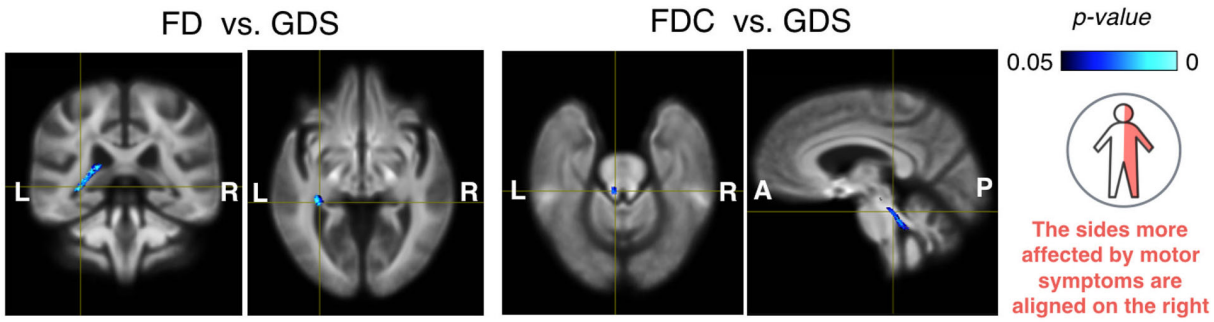


**FIGURE 2** Correlation between fixel-based metrics and clinical evaluations in PD population after aligning laterality of symptom onset (*FBA Study-2*). Significant fiber tracts of fixel-based metrics are overlaid on the group-averaged brain template, and blue color shows negative correlations

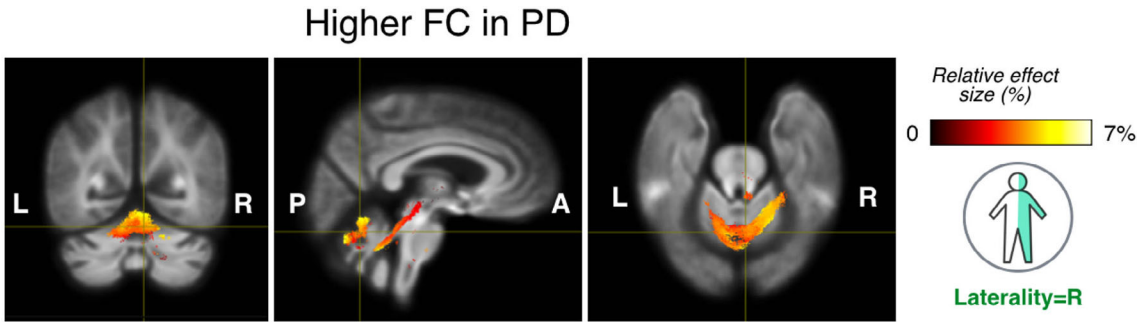


**FIGURE 3** Comparison of fixel-based metrics between right-dominant PD and healthy groups after (*FBA Study-3*). Significant fiber tracts of fixel-based metrics are overlaid on the group-averaged brain template. The fiber tracts are colored by the percentage of effect size in PD group relative to the healthy group mean

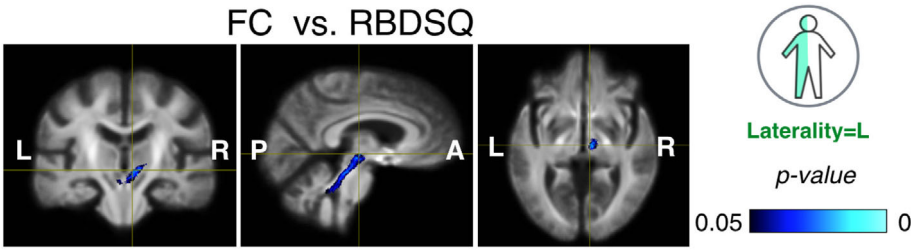


**FIGURE 4** Correlation between fixel-based metrics and RBDSQ in left-dominated PD cohorts (*FBA Study 4*). Significant fiber tracts of fixel-based metrics are overlaid on the group-averaged brain template, and blue color shows negative correlations

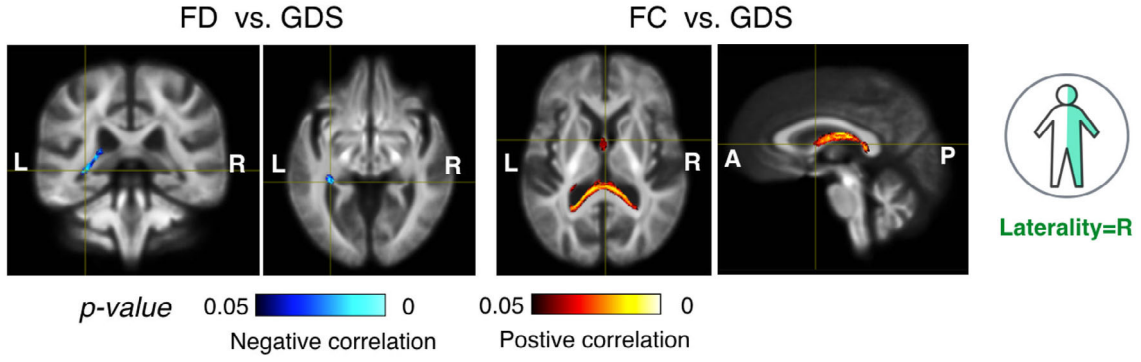


**FIGURE 5** Correlation between fixel-based metrics and clinical evaluations in right-dominated PD cohorts (*FBA Study 4*). Significant fiber tracts of fixel-based metrics are overlaid on the group-averaged brain template

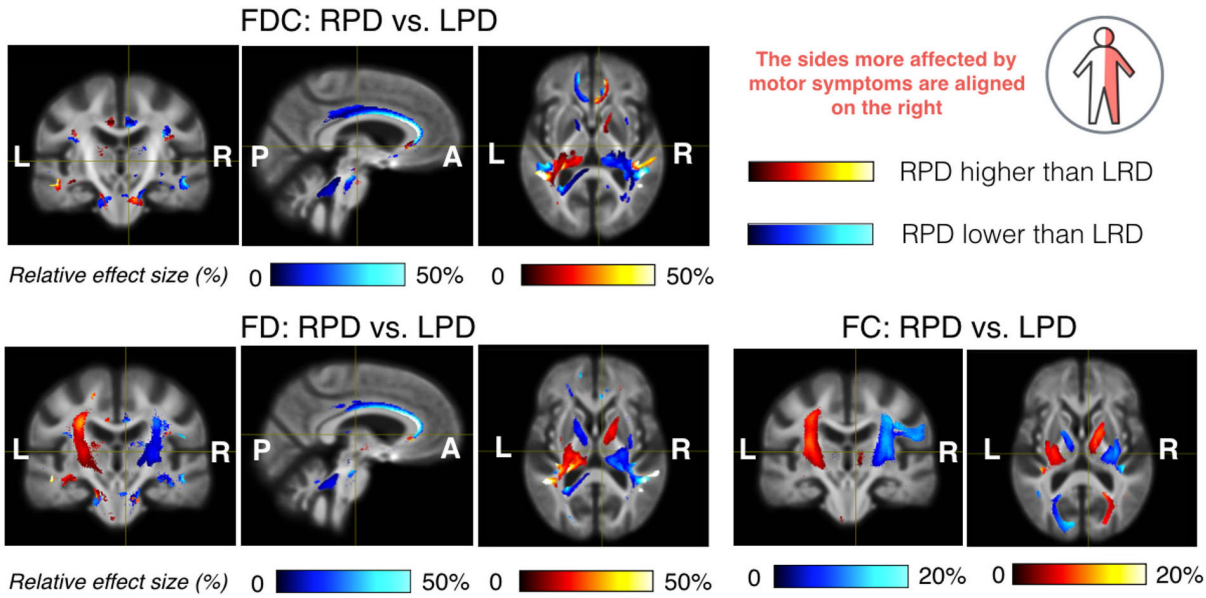


**FIGURE 6** Comparison of fixel-based metrics (FC, FD, and FDC) between RPD and LPD groups after aligning laterality of symptom onset (*FBA Study-5*). Significant fiber tracts of fixel-based metrics (FWE-corrected $p < .05$) are overlaid on the group-averaged brain template, and the fiber tracts are colored by the percentage of effect size in RPD group relative to the LPD group mean. In each image group, the cross-hair points at the same location

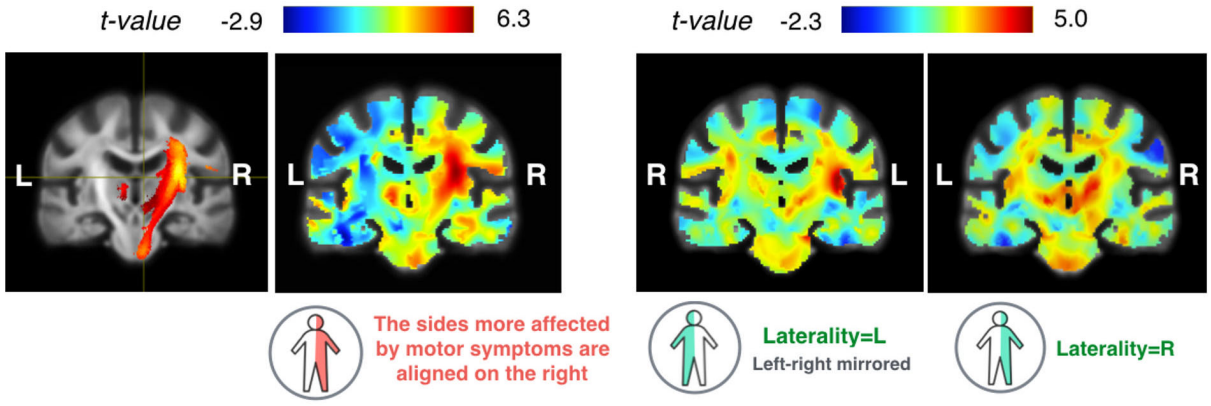


**FIGURE 7** Demonstration of *t*-values from testing the hypothesis that the FC values are higher in PD cohorts than healthy controls in FBA *Study 1* and *3*. From left to right: a coronal slice of the significant fixels from Figure 1, the corresponding *t*-value map from *Study 1*, and the corresponding *t*-value maps from *Study 3* with respect to LPD and RPD sub-cohorts. For easy visual comparison, different *t*-value windows are used between studies, and that of the LPD sub-cohort was left–right mirrored

peduncle, left cingulum, and right forceps minor. For both FD and FDC, the reversed trend mirrored to the opposite side.

Finally, to inspect our approach of aligning the side of symptoms onset, in Figure 7, we illustrate the t-value maps from testing the hypothesis that the FC values are higher in the PD group than the healthy controls in *FBA Study 1 and 3*. In the figure, the coronal slice from Figure 1 demonstrating significant FC alteration in motor-function-related tracts is shown with the corresponding *t*-value maps from the two studies. Note that for easy visual comparison, the *t*-value map for the LPD group is left–right mirrored, and different t-value windows are used between studies.

## 3.2 | Voxel-based analysis

The results of voxel-based analysis are shown in Figures 8–12. Similar to FBA, the effect size as a percentage relative to the healthy control mean was used to color the regions with significant differences between PD and healthy groups. When comparing LPD and RPD cohorts, the significant regions were shown with the effect size as a percentage relative to the LPD mean. For the rest of experimental results, the corresponding FWE corrected *p*-values were used to color the significant tracts.

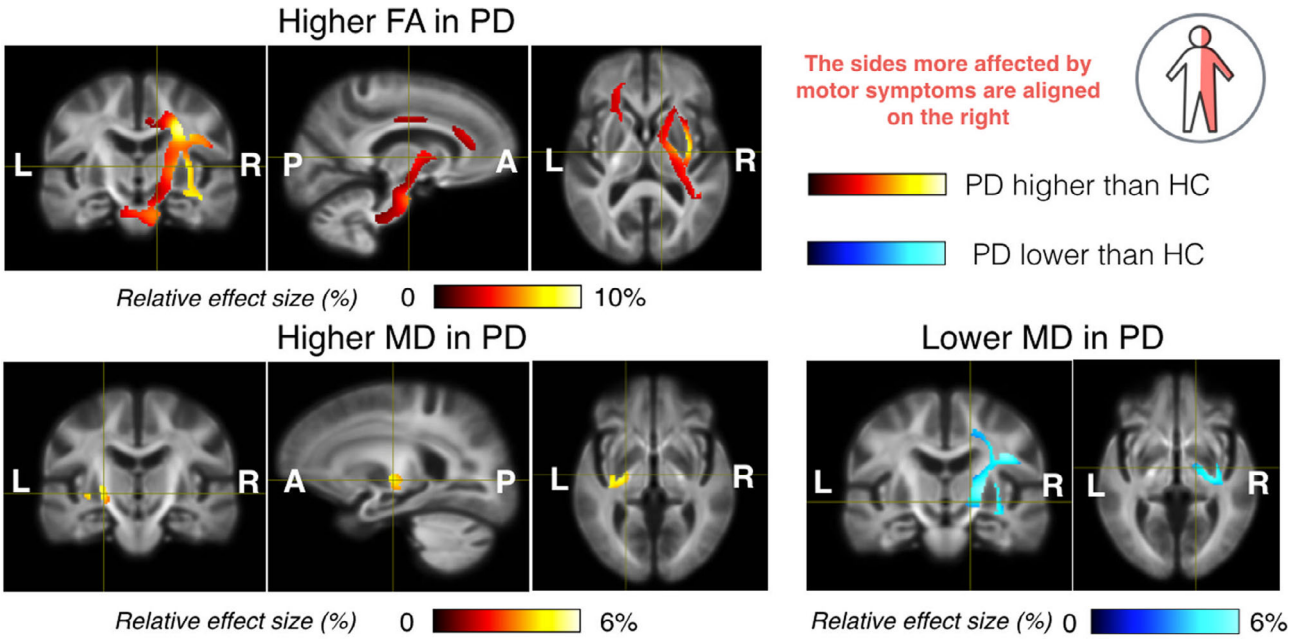


**FIGURE 8** Comparison of fractional anisotropy (FA) and mean diffusivity (MD) between PD and healthy groups after aligning laterality of symptom onset (*VBA Study 1*). Significant clusters of DTI metrics are overlaid on the group-averaged brain template, and are colored by the percentage of effect size in PD group relative to the healthy group mean. In each image group, the cross-hair points at the same location

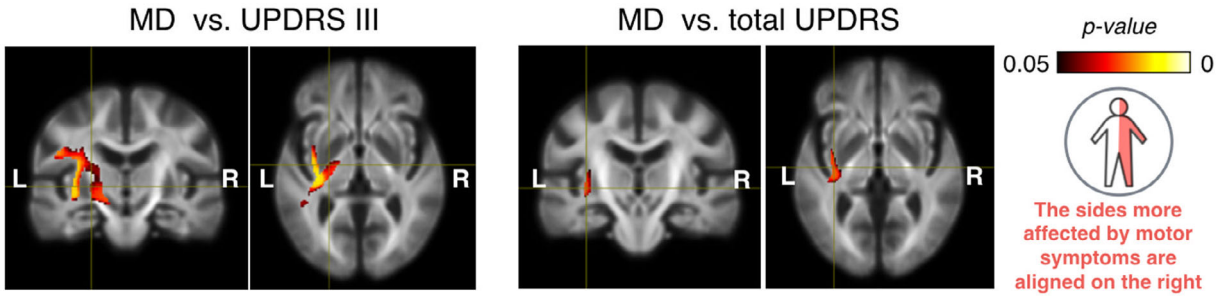


**FIGURE 9** Positive correlation between DTI metrics (FA and MD) and clinical evaluations in PD population after aligning laterality of symptom onset (*VBA Study 2*). Significant regions are overlaid on the group-averaged brain template

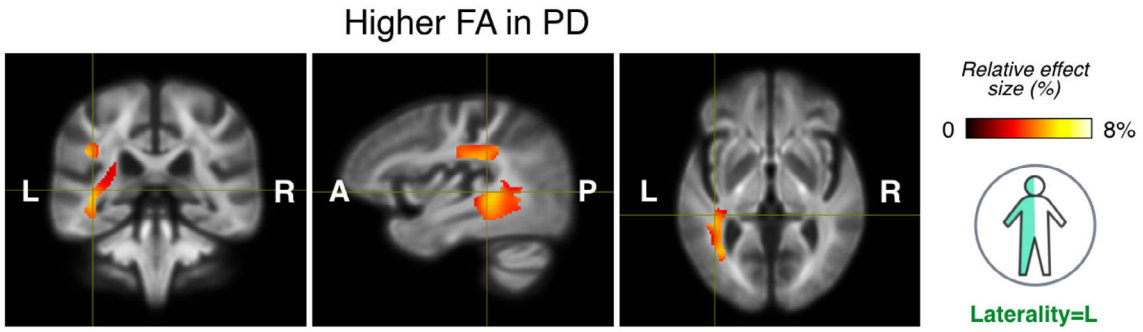


**FIGURE 10** Comparison of FA values between PD and healthy groups in the left-dominant PD cohort (*VBA Study 3*). Significant regions are overlaid on the group-averaged brain template, and are colored by the percentage of effect size in PD group relative to the healthy group mean

We evaluated FA and MD in PD patients against those of healthy controls in *VBA Study 1*, after aligning the symptom dominant side to the right-side of the body. The results are shown in Figure 8. Compared with healthy subjects, PD patients had a widespread region with larger FA primarily within the right hemisphere, which was ipsilateral to the dominant side of motor symptoms. The white matter

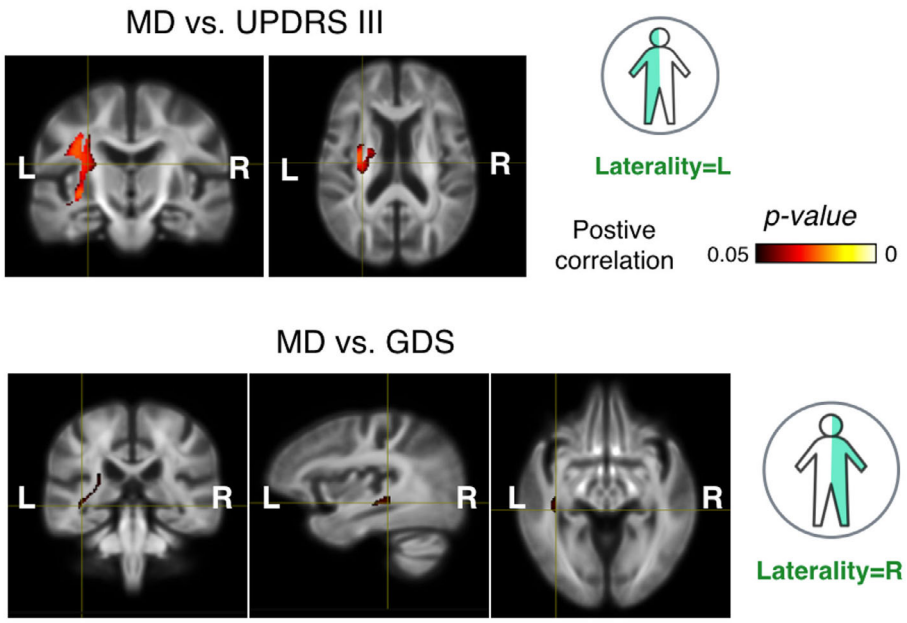


**FIGURE 11** Correlation between DTI metrics (FA and MD) and clinical evaluations in left-dominant and right-dominated PD cohorts (*VBA Study 4*). Significant regions are overlaid on the group-averaged brain template

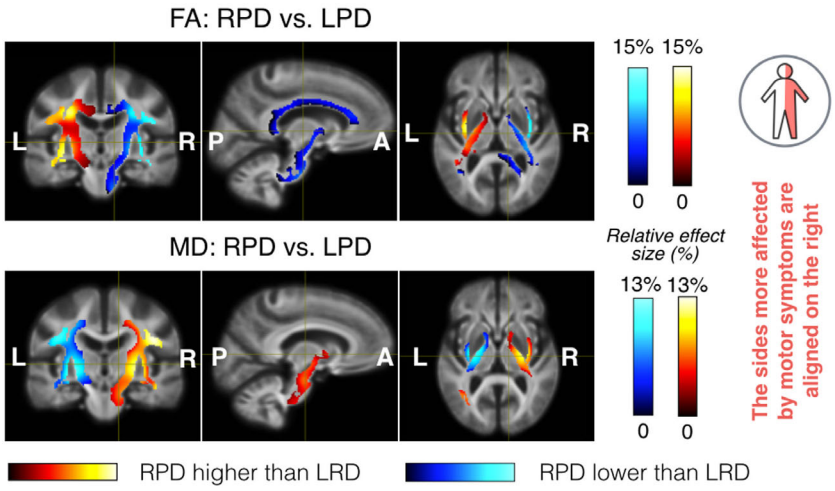


**FIGURE 12** Comparison of fractional anisotropy (FA) and mean diffusivity (MD) between RPD and LPD groups after aligning laterality of symptom onset (*VBA Study 5*). Significant regions (FWE-corrected $p < .05$) are overlaid on the group-averaged brain template, and the regions are colored by the percentage of effect size in RPD group relative to LPD group mean. In each image group, the cross-hair points at the same location

tracts with higher FA included the right superior longitudinal fasciculus (SLF), posterior limb of internal capsule, cerebellar peduncle, cingulum, superior corona radiata, external capsule, and middle cerebral peduncle. In addition, there was also greater FA in the left anterior corona radiata, and reduction of MD in the patients occurred in the right internal capsule and superior corona radiata. On the other hand, elevated MD in PD can be found in small regions within the left posterior limb of internal capsule and external capsule. With *VBA Study 2* (see Figure 9), white matter fiber deterioration in terms of higher MD in the left external capsule, superior corona radiata, and SLF was linked to worsening of UPDRS-III scores. Furthermore, the left external capsule had higher MD that was correlated with the total UPDRS assessment.

When comparing left-dominant and right-dominant PD groups with the healthy controls (*VBA Study 3*), as demonstrated in Figure 10, we found greater FA in the left posterior thalamic radiata and superior corona radiata in the LPD cohort while no differences were detected between the RPD group and healthy controls. With *VBA Study 4*, several trends were observed in Figure 11. In the LPD sub-cohort, the UPDRS-III score was associated with higher MD values in the left internal capsule, superior corona radiata, and external capsule. For RPD, MD values in the retrolenticular part of the internal capsule in the left hemisphere are positively correlated with GDS.

We compared the DTI-metrics between LPD and RPD cohorts in *VBA Study 5* with the scans of LPD subjects left–right mirrored. As shown in Figure 12, similar to *FBA Study 5*, the regions with higher and lower measures in RPD than LPD were generally symmetric between hemispheres. Compared with LPD, RPD had higher FA values in the internal capsule, external capsule, cingulum, and superior corona radiata in the left hemisphere. On the other hand, the MD values were higher in the internal capsule, external capsule, and superior corona radiata in the right hemisphere. For FA and MD, the reversed trend mirrored to the opposite side.

## 4 | DISCUSSION

In *FBA Study 1*, where scans of LPD patients were flipped in the left–right direction, higher FC and FDC were observed in the right hemisphere for PD patients compared with healthy subjects, primarily in white matter tracts that are associated with motor control. The same trend is replicated in the elevated FA and lower MD in the same hemisphere from *VBA Study 1*. These results confirmed the observation in previous studies (Li et al., 2020; Mole et al., 2016), where higher FD and FA in CST were detected in PD compared with HC. However, while these studies suggested bilateral changes, we observed primarily unilateral alterations, potentially due to the consideration of symptom laterality onset. On the other hand, degeneration of white matter was also shown with both fixel-based and DTI metrics in the hemisphere that is more affected by motor dysfunction. Interestingly, while FBA identified the cingulum, which is more involved in the limbic system, VBA revealed regions that are more relevant to motor functions. When inspecting the clinical symptoms within the PD group (*Study 2*), with the same strategy of aligning the clinical laterality onset, the relevant white matter tracts/regions that were associated with the clinical symptoms were identified in the left hemisphere. This is not surprising for UPDRS III and total UPDRS assessments in VBA studies, but further investigation is needed regarding nonmotor symptoms (i.e., GDS) in FBA studies and the relationship to clinical laterality.

To better elucidate the distinct trends in LPD and RPD cohorts, the analyses in *Study 3* and *Study 4* examined these sub-groups separately. In *FBA Study 3* for RPD patients, elevated FC was observed in the right SCP, which is consistent with *FBA Study 1*, and the cerebellum. Previous studies (Sweet et al., 2014; Wu & Hallett, 2013) have revealed the role of cerebellum and the related neural pathways in motor dysfunctions of PD. As the RPD group have less severe clinical symptoms on average than LPD, whether the observed trend is specific to RPD or the disease progression stage will require further investigation. In *VBA Study 3* with LPD patients, regions with strengthened white matter integrity were found in the left hemisphere in PD patients. This trend is consistent with *Study 1*, but the higher FA in the posterior thalamic radiata was unique to LPD. When associating white matter health with nonmotor symptoms of sleep disturbance and depression in *VBA* and *FBA Study 4*, both positive and negative correlations have been identified, potentially implying a complex mechanism for nonmotor symptoms. In contrast to the trend in *VBA Study 2*, there was a positive correlation between the UPDRS-III scores and the MD values in the left hemisphere for LPD. While lacking statistical significance between LPD and RPD, the mean UPDRS III and total UPDRS were higher in LPD than RPD. As revealed in previous literature (Li et al., 2020; Rau et al., 2019; Sarasso et al., 2020), the alterations of white matter integrity measures in PD is complex and nonlinear. Although initial improvement in the measures can occur, eventually deterioration will take place as the disease progresses. The observed correlation may be a result from the deterioration of motor functions on the less dominant side as the disease progresses. In general, FBA and VBA both offer insights of disease-related white matter changes, but since FBA emphasizes tract-specific measures, and VBA with DTI metrics produce clustered regions, the identified regions with statistical significance do not necessarily overlap with each other. Compared with FBA, VBA with DTI metrics is more sensitive in identifying associated brain regions with respect to clinical symptoms, despite the drawbacks in the difficulty in resolving crossing fibers.

We compared LPD and RPD in *FBA and VBA Study 5*, where the motor symptom-dominant side was aligned to the right side of the body. The white matter tracts, including CST, SCP, cingulum that were identified in *FBA Study 1* showed higher fixel-based metrics for RPD in the hemisphere that is more affected and lower values in the other. The same trend was also shown with DTI-metrics, where the RPD group had better white matter integrity as suggested by higher FA and lower MD than the LPD group in the more affected hemisphere, and the opposite trend was generally observed in the mirrored tracts on the other side. We hypothesize that the observations may come from two potential sources. First, LPD patients had more severe symptoms on average, which may reduce the integrity of relevant white matter tracts in the symptom-dominant side while improving the white matter integrity measures on the opposite side in early PD. Second, as LPD and RPD can have different prognoses (Baumann et al., 2014; Munhoz et al., 2013), the inherent differences between sub-cohorts may have also contributed to the observations. Future longitudinal studies with diffusion imaging will better elucidate the observed differences, but are out of the scope of this study.

In common with the two existing FBA studies on PD progression (Li et al., 2020; Rau et al., 2019), both of which used 3 T data, we have identified the splenium of CC, CST, SCP, cingulum, and fornix as regions that are affected by the disease. However, within these tracts, the specific trends in fixel-based measures do not always agree among previous studies (Li et al., 2020; Rau et al., 2019) and ours. For example, Rau et al. (2019) discovered that the UDPRS assessments, including UPDRS III and total UPDRS, are positively correlated with FC in the body of CC, but Li et al. (2020) found a negative association between FD values in the same structure and UPDRS III. In our cohorts, no significant results were revealed for UPDRS evaluations and fixel-based measures. Furthermore, Li et al. (2020) associated reduced FD in the CC with depression while our results showed higher FC in the splenium of CC with depression in RPD. Previously, Pelizzari et al. (2020) have also compared DTI metrics between PD patients with unilateral symptoms and healthy controls. Different from our results, they found widespread white matter integrity reduction in terms of higher MD in RPD but not in LPD. These differences may originate from several sources, such as variations in imaging protocols (e.g., multishell vs. single-shell and different *b*-values), cohort size, and patient heterogeneity. Notably, these recent studies included patients at slightly more advanced disease stages (H&Y stages 1–3) than our PD cohort (H&Y stages 1–2). Another potential contributor to the difference is the influence of dopaminergic therapy. This factor may alter white matter properties in addition to the disease itself, but is often overlooked in most studies (Zhang & Burock, 2020), including those mentioned in this paragraph. As the influence of drug therapy is still poorly understood, investigation of tissue changes in drug-naïve

PD can provide a baseline to clarify the relationship between brain plasticity and PD treatment.

Higher FA and lower MD within white matter, especially the CST, have been reported previously in early PD (Cousineau et al., 2017; Wen et al., 2018; Zhang & Burock, 2020). Furthermore, several groups have also revealed an initial improvement of white matter microstructural measures (Li et al., 2020; Rau et al., 2019; Zhang & Burock, 2020) with an eventual decline, rather than a monotonic degeneration. Our results corroborate these findings. An increase in FC may be interpreted as widening of extra-axon space or improved organization of axons (Raffelt et al., 2017) while FDC measures the joint impacts from FC and FD. However, as the more recent FBA-based metrics are relative measures, their interpretation requires further investigation in conjunction with histological data and other quantitative imaging techniques. To explain the higher FA observed in their study in early PD, Mole et al. (2016) suggested the neurodegenerative and neuroplastic models. While the first explains the elevated FA as a primary pathogenic consequence of altered pallido-thalamic activity in PD, the second proposes it as an adaptive structural reorganization towards abnormal dopaminergic modulation. As FA was suggested to be more linked to axonal package density than myelination (Winston, 2012) in the neurodegenerative model, the lack of elevated FD in PD in our study presented weak support for it. However, further caution and investigation are needed to interpret the observations as a result of neural compensation.

The development and progression of PD is complex and nonlinear (Li et al., 2020; Rau et al., 2019; Sarasso et al., 2020), often with the motor symptoms initiating unilaterally and progressing to both sides in more advanced stages. This is expected to induce differential patterns of tissue changes, and thus brain connectivity alterations between the left and right hemispheres. However, most PD-related investigations on microstructural and macrostructural changes do not consider the laterality of the dominant symptoms, especially when many focus on early stages of PD. Such an approach may reduce the sensitivity for detecting disease-related brain regions, or reporting bilateral changes instead of potentially unilateral changes, possibly contributing to inconsistent conclusions in the literature. Our analyses were conducted with strategies that fully account for laterality. In the first strategy, the sides with more severe symptoms were mapped to the right for all subjects. This allows the entire PD population to be included, thus boosting the statistical power to detect relevant trends with a clinical DTI protocol. As a result, we were able to reveal laterality-dependent microstructural alterations in drug-naïve de novo PD patients, which were not demonstrated previously. In the second strategy, sub-groups of LPD and RPD patients were analyzed separately. This approach helped confirm the insights related to laterality of symptoms onset, and provided complementary tissue characterizations that are specific to each sub-group. From Figure 7, we can see that despite the fact that the LPD and RPD sub-cohorts did not show statistically significant trends in the same white matter tracts, we can still observe a similar trend of higher *t*-values in the relevant regions from the hemisphere that is less affected by PD, across the three maps. This confirmed the validity of our approach to inspect the white matter tissue properties subject to clinical laterality.

The described studies still have a number of limitations. First, the analyses employed clinical single-shell DTI protocols at 3 T (64 gradient directions, $b = 1{,}000$ s/mm$^2$), and thus the data quality can be lower than those from multishell protocols with higher *b*-values (Rau et al., 2019; Zarkali et al., 2020), which offer superior signal-to-noise ratio and angular contrast-to-noise ratio to better resolve fiber crossings. In FBA, this may affect the interpretation of FD and FDC, and may have partially contributed to the discrepancies between our results and those of Rau et al. (2019). Future FBA studies with DWI data using higher *b*-values ($b > 2{,}000$ s/mm$^2$) and a large PD cohort are recommended, and should be instrumental to confirm the presented results. Note that Li et al. (2020) also used single-shell DWI data with $b = 1{,}000$ s/mm$^2$ in their FBA study of PD. The discrepancies between our results and theirs may come from multiple factors as mentioned earlier. For FBA, we employed the recent single-shell multitissue CSD algorithm to accommodate the scanning protocol, and showed that meaningful results can still be obtained with single-shell DWI scans. Second, as the DWI scans in the PPMI database do not have matching scans with opposing phase encoding directions, susceptibility-induced distortion was corrected through nonlinear registration between the corresponding $B_0$ and T2w MRIs. Although this type of approach was used previously (Ardekani & Sinha, 2005), it may limit the accuracy of the analyses, particularly in regions with more severe distortions (e.g., orbital frontal and temporal lobes). Lastly, part of our study aligned the clinical laterality onset to the right side for analysis. In addition to the asymmetry potentially introduced by the disease, inherent asymmetry of the brain may have also contributed to the observations. To inspect the potential difference, LPD and RPD sub-groups were analyzed separately, and similar trend was found to the studies that align the dominant symptom side. However, further quantification of the influence from inherent brain asymmetry on PD is beyond the scope of the current investigation, and will be explored in detail in the future study.

Recently, white matter hyper-intensity (WMH) lesion load has been linked to increased future cognitive decline in de novo PD (Dadar et al., 2018). As an assessment of white matter integrity, FBA-based metrics at each voxel are derived from the FOD map, and the presence of WMH lesions can be reflected in local reduction of these measures. For FBA, an average tractogram was used in statistical inference (Raffelt et al., 2015), and is generated from a population-average FOD template using a whole-brain probabilistic tractography algorithm (Tournier et al., 2010). In our studies, we did not identify visible hypo-intensity spots in the FOD template or evident artifacts in the tractogram. Previously, FBA has been employed in PD (Li et al., 2020; Rau et al., 2019) and Alzheimer's disease (Mito et al., 2018) that can be complicated by WMH. Although the present investigation did not account for lesions, future work can benefit from precise modeling of the effects of WMH through accurate lesion segmentation algorithms.

## 5 | CONCLUSION

In this study, we present the first investigation that characterizes white matter integrity with the consideration of symptom laterality in a large drug-naïve de novo PD cohort, using complementary DTI and FBA measures. In addition to revealing tissue alterations between PD and healthy subjects, we demonstrated that both motor and non-motor clinical assessments were correlated with different DTI and FBA measures within white matter pathways. The findings suggest that the disease gives rise to both tissue degeneration and potential re-organization in the early stage, and the impacts may be subject to the laterality of the motor symptoms. In the meanwhile, the results also showed differences between LPD and RPD cohorts that may be a result of the respective disease trajectories (Baumann et al., 2014) and potential disparity in disease severity between the two groups. As the first FBA investigation with a drug naïve PD population, the insights are instrumental in understanding the progression of the disease and potentially inform the future exploration regarding the interplay between disease-related brain tissue changes and drug therapy. To depict a richer picture of the disease, future longitudinal studies will help fully characterize the trajectory of PD-related white matter changes as a potential biomarker for improved prognosis and treatments.

### ACKNOWLEDGMENTS

The work is supported by the BrainsCAN and CIHR fellowships for Y. Xiao. The authors would like to thank Dr. Thijs Dhollander for his insightful discussion on MRtrix software and fixel-based analysis.

### CONFLICT OF INTEREST

The authors declare no conflicts of interest.

### DATA AVAILABILITY STATEMENT

The data that support the findings of the study are publicly available at www.ppmi-info.org. PPMI-a public-private partnership-is funded by the Michael J. Fox Foundation for Parkinson's Research and funding partners, including AbbVie, Avid, Biogen, Bristol-Myers Squibb, Covance, GE Healthcare, Genentech, GlaxoSmithKline, Lilly, Lundbeck, Merck, Meso Scale Discovery, Pfizer, Piramal, Roche, Sanofi Genzyme, Servier, Teva, and UCB.

### ORCID

*Yiming Xiao* https://orcid.org/0000-0002-0962-3525
*Terry M. Peters* https://orcid.org/0000-0003-1440-7488
*Ali R. Khan* https://orcid.org/0000-0002-0760-8647

### REFERENCES

Andersson, J. L. R., & Sotiropoulos, S. N. (2016). An integrated approach to correction for off-resonance effects and subject movement in diffusion MR imaging. *NeuroImage*, *125*, 1063–1078.

Ardekani, S., & Sinha, U. (2005). Geometric distortion correction of high-resolution 3 T diffusion tensor brain images. *Magnetic Resonance in Medicine*, *54*(5), 1163–1171.

Atkinson-Clement, C., Pinto, S., Eusebio, A., & Coulon, O. (2017). Diffusion tensor imaging in Parkinson's disease: Review and meta-analysis. *Neuroimage: Clinical*, *16*, 98–110.

Baumann, C. R., Held, U., Valko, P. O., Wienecke, M., & Waldvogel, D. (2014). Body side and predominant motor features at the onset of Parkinson's disease are linked to motor and nonmotor progression. *Movement Disorders*, *29*(2), 207–213.

Choy, S. W., Bagarinao, E., Watanabe, H., Ho, E. T. W., Maesawa, S., Mori, D., … Sobue, G. (2020). Changes in white matter fiber density and morphology across the adult lifespan: A cross-sectional fixel-based analysis. *Human Brain Mapping*, *41*(12), 3198–3211.

Cousineau, M., Jodoin, P. M., Morency, F. C., Rozanski, V., Grand'Maison, M., Bedell, B. J., & Descoteaux, M. (2017). A test-retest study on Parkinson's PPMI dataset yields statistically significant white matter fascicles. *Neuroimage: Clinical*, *16*, 222–233.

Dadar, M., Zeighami, Y., Yau, Y., Fereshtehnejad, S. M., Maranzano, J., Postuma, R. B., … Collins, D. L. (2018). White matter hyperintensities are linked to future cognitive decline in de novo Parkinson's disease patients. *Neuroimage: Clinical*, *20*, 892–900.

Dhollander, T., Raffelt, D., & Connelly, A. (2016). Unsupervised 3-tissue response function estimation from single-shell or multi-shell diffusion MRI data without a co-registered T1 image. ISMRM Workshop on Breaking the Barriers of Diffusion MRI.

Egorova, N., Dhollander, T., Khlif, M. S., Khan, W., Werden, E., & Brodtmann, A. (2020). Pervasive white matter fiber degeneration in ischemic stroke. *Stroke*, *51*(5), 1507–1513.

Eskildsen, S. F., Coupe, P., Fonov, V., Manjon, J. V., Leung, K. K., Guizard, N., … Alzheimer's Disease Neuroimaging Initiative. (2012). BEaST: Brain extraction based on nonlocal segmentation technique. *NeuroImage*, *59*(3), 2362–2373.

Ji, G. J., Ren, C., Li, Y., Sun, J., Liu, T., Gao, Y., … Wang, K. (2019). Regional and network properties of white matter function in Parkinson's disease. *Human Brain Mapping*, *40*(4), 1253–1263.

Li, Y., Guo, T., Guan, X., Gao, T., Sheng, W., Zhou, C., … Huang, P. (2020). Fixel-based analysis reveals fiber-specific alterations during the progression of Parkinson's disease. *Neuroimage: Clinical*, *27*, 102355.

Lyon, M., Welton, T., Varda, A., Maller, J. J., Broadhouse, K., Korgaonkar, M. S., … Grieve, S. M. (2019). Gender-specific structural abnormalities in major depressive disorder revealed by fixel-based analysis. *Neuroimage: Clinical*, *21*, 101668.

Manjon, J. V., Coupe, P., Marti-Bonmati, L., Collins, D. L., & Robles, M. (2010). Adaptive non-local means denoising of MR images with spatially varying noise levels. *Journal of Magnetic Resonance Imaging*, *31*(1), 192–203.

Mito, R., Raffelt, D., Dhollander, T., Vaughan, D. N., Tournier, J. D., Salvado, O., … Connelly, A. (2018). Fibre-specific white matter reductions in Alzheimer's disease and mild cognitive impairment. *Brain*, *141*(3), 888–902.

Mole, J. P., Subramanian, L., Bracht, T., Morris, H., Metzler-Baddeley, C., & Linden, D. E. (2016). Increased fractional anisotropy in the motor tracts of Parkinson's disease suggests compensatory neuroplasticity or selective neurodegeneration. *European Radiology*, *26*(10), 3327–3335.

Mori, S., Oishi, K., Jiang, H., Jiang, L., Li, X., Akhter, K., … Mazziotta, J. (2008). Stereotaxic white matter atlas based on diffusion tensor imaging in an ICBM template. *NeuroImage*, *40*(2), 570–582.

Munhoz, R. P., Espay, A. J., Morgante, F., Li, J. Y., Teive, H. A., Dunn, E., … Litvan, I. (2013). Long-duration Parkinson's disease: Role of lateralization of motor features. *Parkinsonism & Related Disorders*, *19*(1), 77–80.

Nichols, T. E., & Holmes, A. P. (2002). Nonparametric permutation tests for functional neuroimaging: A primer with examples. *Human Brain Mapping*, *15*(1), 1–25.

Pelizzari, L., Di Tella, S., Lagana, M. M., Bergsland, N., Rossetto, F., Nemni, R., & Baglio, F. (2020). White matter alterations in early Parkinson's disease: Role of motor symptom lateralization. *Neurological Sciences*, *41*(2), 357–364.

Raffelt, D. A., Smith, R. E., Ridgway, G. R., Tournier, J. D., Vaughan, D. N., Rose, S., … Connelly, A. (2015). Connectivity-based fixel enhancement: Whole-brain statistical analysis of diffusion MRI measures in the presence of crossing fibres. *NeuroImage*, *117*, 40–55.

Raffelt, D. A., Tournier, J. D., Smith, R. E., Vaughan, D. N., Jackson, G., Ridgway, G. R., & Connelly, A. (2017). Investigating white matter fibre density and morphology using fixel-based analysis. *Neuroimage*, *144*, 58–73.

Rau, Y. A., Wang, S. M., Tournier, J. D., Lin, S. H., Lu, C. S., Weng, Y. H., … Wang, J. J. (2019). A longitudinal fixel-based analysis of white matter alterations in patients with Parkinson's disease. *Neuroimage: Clinical*, *24*, 102098.

Sarasso, E., Agosta, F., Piramide, N., & Filippi, M. (2020). Progression of grey and white matter brain damage in Parkinson's disease: A critical review of structural MRI literature. *Journal of Neurology*. https://doi.org/10.1007/s00415-020-09863-8

Scherfler, C., Seppi, K., Mair, K. J., Donnemiller, E., Virgolini, I., Wenning, G. K., & Poewe, W. (2012). Left hemispheric predominance of nigrostriatal dysfunction in Parkinson's disease. *Brain*, *135*, 3348–3354.

Shang, S., Wu, J., Zhang, H., Chen, H., Cao, Z., Chen, Y. C., & Yin, X. (2020). Motor asymmetry related cerebral perfusion patterns in Parkinson's disease: An arterial spin labeling study. *Human Brain Mapping*, *42*, 298–309.

Smith, R. E., Tournier, J. D., Calamante, F., & Connelly, A. (2013). SIFT: Spherical-deconvolution informed filtering of tractograms. *NeuroImage*, *67*, 298–312.

Sweet, J. A., Walter, B. L., Gunalan, K., Chaturvedi, A., McIntyre, C. C., & Miller, J. P. (2014). Fiber tractography of the axonal pathways linking the basal ganglia and cerebellum in Parkinson disease: Implications for targeting in deep brain stimulation. *Journal of Neurosurgery*, *120*(4), 988–996.

Tournier, J. D., Calamante, F., & Connelly, A. (2010). *Improved probabilistic streamlines tractography by 2nd order integration over fibre orientation distributions*. Proceedings of the International Society for Magnetic Resonance in Medicine.

Tournier, J. D., Smith, R., Raffelt, D., Tabbara, R., Dhollander, T., Pietsch, M., … Connelly, A. (2019). MRtrix3: A fast, flexible and open software framework for medical image processing and visualisation. *NeuroImage*, *202*, 116137.

Tustison, N. J., Avants, B. B., Cook, P. A., Zheng, Y., Egan, A., Yushkevich, P. A., & Gee, J. C. (2010). N4ITK: Improved N3 bias correction. *IEEE Transactions on Medical Imaging*, *29*(6), 1310–1320.

Veraart, J., Novikov, D. S., Christiaens, D., Ades-Aron, B., Sijbers, J., & Fieremans, E. (2016). Denoising of diffusion MRI using random matrix theory. *NeuroImage*, *142*, 394–406.

Wallace, E. J., Mathias, J. L., Ward, L., Fripp, J., Rose, S., & Pannek, K. (2020). A fixel-based analysis of micro- and macro-structural changes to white matter following adult traumatic brain injury. *Human Brain Mapping*, *41*(8), 2187–2197.

Wen, M. C., Heng, H. S. E., Lu, Z., Xu, Z., Chan, L. L., Tan, E. K., & Tan, L. C. S. (2018). Differential white matter regional alterations in motor subtypes of early drug-naive Parkinson's disease patients. *Neurorehabilitation and Neural Repair*, *32*(2), 129–141.

Winston, G. P. (2012). The physical and biological basis of quantitative parameters derived from diffusion MRI. *Quantitative Imaging in Medicine and Surgery*, *2*(4), 254–265.

Wu, T., & Hallett, M. (2013). The cerebellum in Parkinson's disease. *Brain*, *136*, 696–709.

Xiao, Y., Jannin, P., D'Albis, T., Guizard, N., Haegelen, C., Lalys, F., … Collins, D. L. (2014). Investigation of morphometric variability of subthalamic nucleus, red nucleus, and substantia nigra in advanced Parkinson's disease patients using automatic segmentation and PCA-based analysis. *Human Brain Mapping*, *35*(9), 4330–4344.

Zarkali, A., McColgan, P., Leyland, L. A., Lees, A. J., Rees, G., & Weil, R. S. (2020). Fiber-specific white matter reductions in Parkinson hallucinations and visual dysfunction. *Neurology*, *94*(14), e1525–e1538.

Zhang, Y., & Burock, M. A. (2020). Diffusion tensor imaging in Parkinson's disease and Parkinsonian syndrome: A systematic review. *Frontiers in Neurology*, *11*, 531993.

**How to cite this article:** Xiao, Y., Peters, T. M., & Khan, A. R. (2021). Characterizing white matter alterations subject to clinical laterality in drug-naïve de novo Parkinson's disease. *Human Brain Mapping*, *42*(14), 4465–4477. https://doi.org/10.1002/hbm.25558